

## Collisional cooled Ps emitted into vacuum from silica-based porous materials: experiment to measure the Ps cooling time

This content has been downloaded from IOPscience. Please scroll down to see the full text.

2015 J. Phys.: Conf. Ser. 618 012039

(<http://iopscience.iop.org/1742-6596/618/1/012039>)

View [the table of contents for this issue](#), or go to the [journal homepage](#) for more

Download details:

IP Address: 193.205.210.41

This content was downloaded on 26/06/2015 at 06:46

Please note that [terms and conditions apply](#).

## Collisional cooled Ps emitted into vacuum from silica-based porous materials: experiment to measure the Ps cooling time

S Mariazzi<sup>1</sup>, L Di Noto<sup>2,4</sup>, G Nebbia<sup>3</sup> and R S Brusa<sup>2</sup>

<sup>1</sup>Stefan-Meyer-Institut für subatomare Physik, Boltzmannngasse 3, 1090 Vienna, Austria

<sup>2</sup>Department of Physics, University of Trento and INFN-TIFPA, Via Sommarive 14, 38123 Povo, Trento, Italy

<sup>3</sup>INFN Padova, Via Marzolo 8, 35131 Padova, Italy

<sup>4</sup>Present address: Dipartimento di Fisica, Università degli Studi e INFN Sez. Genova, Via Dodecanneso 33, 16145 Genova, Italy.

E-mail: brusa@science.unitn.it

**Abstract.** In recent experiments on positronium time of flight (Ps-TOF) we have studied emission of cooled and thermalized Ps into vacuum from oxidized nanochannels synthesized in silicon. Ps cools down through collisions with the walls of the channels before exiting into vacuum. An important unknown parameter in the Ps-TOF measurements is the permanence time in the medium, i.e. the Ps cooling time before emission into vacuum. In this paper we describe an experiment that allows us to estimate the cooling time of Ps by analyzing the Ps-TOF spectra of cool Ps at three different distances from the sample.

### 1. Introduction

There is a demand for cool Ps in vacuum for spectroscopy experiments [1, 2] and for the production of anti-hydrogen beams through the charge exchange reaction between antiprotons and Ps excited in Rydberg states [3]. An efficient way of cooling Ps is to form it by injecting  $e^+$  with energy ( $E_+$ ) of some keV in porous silica materials with porosities open towards the vacuum [4]. Ps is emitted from the bulk into the pores with energy from  $\sim 1$  eV to  $\sim 3$  eV, then it reduces its kinetic energy by collisions with the walls of the pores and a cooled fraction escapes into vacuum [4]. In porous materials, with 2.7 nm pores size, a Ps kinetic energy of 42 meV was measured via Doppler broadening of the  $1^3S-2^3P$  transition in the laser direction [5]. The incomplete thermalization was consistent with the energy of Ps quantum confined in the pores [6]. The limit imposed by quantum confinement was circumvented forming Ps in oxidized nanochannels with lateral dimensions of few nanometers [7] and Ps was found to escape with thermal energy at sample temperature in the 150-300 K range [8]. Knowledge of the time delay between  $e^+$  implantation and cooled Ps emission (Ps cooling time) is important both for a correct interpretation of the Ps-TOF measurements [9] and for an efficient laser excitation of the Ps bunch [3].

The aim of this paper is to present an experimental method for measuring the Ps cooling time. The Ps-TOF measurements were done at room temperature (RT) in oxidized nanochannels. Only a rough estimation of the cooling time will be given because the poor statistics.



## 2. Experimental

Oxidized nanochannels with diameters in the 5-8 nm range were obtained by electrochemical etching as described in Ref. 7, 8. Nanochannels were produced in the first 2  $\mu\text{m}$  of the silicon sample. Ps-TOF measurement were carried out with a slow continuous positron beam [10] keeping the sample at  $300 \pm 1$  K. The Ps energy component perpendicular to the target surface  $E_{\perp} = (m_0 z_0^2)/t^2$ , where  $m_0$  is the  $e^+$  rest mass and  $z_0$  the distance of the slit center from the target, was derived measuring the time  $t$  between  $e^+$  implantation on the target and the  $\gamma$ -rays of Ps annihilation in flight. The start signal was given by detecting the secondary electrons with two channeltrons, while the stop signals were given by 5 NaI(Tl) detectors arranged in an arc at a radial distance of 130 mm from the sample axis. A 100 mm thick lead shield, with a 5 mm slit was placed in front of the detectors (figure 1). Spectra were measured at three different distances  $z_0$  from the target.

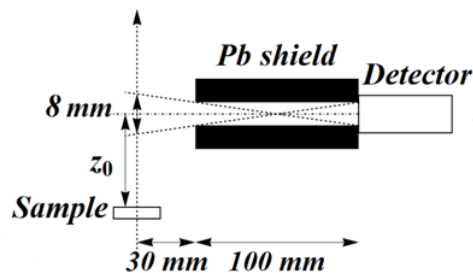


**Figure 1.** Sketch of the Ps-TOF set up.

Both start and stop signals, were combined in a fan-in/fan-out module and  $\sim 10^4$  coincidence events were collected for each spectrum using a time-to-amplitude converter. Details of the Ps-TOF set up can be found in Ref. 11.

In order to evaluate the system resolution and the background a calibration run was performed on a sample made of a Si single-crystal. The resolution function was found to be a Gaussian with 16 ns FWHM by fitting the positron annihilation prompt peak. The Ps-TOF spectra were smoothed through a moving average filtering on 21 channels (0.405 ns/channel). The background due to prompt  $e^+$  annihilations was subtracted and the effect of Ps finite lifetime and permanence in front of the slit was taken into account by the multiplication factor  $e^{t/142\text{ns}}/t$  [12]. The TOF spectra were multiplied by  $t^3$  in order to obtain the energy spectra [12].

## 3. Results and discussion

With the aim of measuring the Ps cooling time when Ps approaches thermal energies, the  $e^+$  implantation energy was increased up to the value of  $E_+$  at which a first fraction of near thermal Ps is emitted. The average positron implantation depth  $\bar{z}$  is related to the positron implantation energy by  $\bar{z} [\text{nm}] = 40/\rho [\text{g}/\text{cm}^3] (E_+ [\text{keV}])^{1.6}$  where  $\rho$  is the sample density [5]. At low  $E_+$  Ps is formed near the surface therefore it does not undergo enough collisions with the nanochannel walls to reach thermal energies. On the contrary, at higher  $E_+$  Ps is formed deeper in the sample and the emission time becomes longer than the thermalization time. The energy spectra obtained by analyzing Ps-TOF spectra measured at  $z_0 = 1$  cm and with  $E_+ = 6$  keV and  $E_+ = 7$  keV are shown in figure 2a-2b (in different scales) and in figure 2c respectively. In figure 2c the spectra measured at  $E_+ = 7$  keV for  $z_0 = 2$  cm and  $z_0 = 3$  cm, are also reported. The energy spectra, in the following, are analyzed up to energies of 150-200 meV since for higher energies the tail of the prompt peak cannot be distinguished from the emission of fast Ps atoms.

The logarithmic spectra were fitted by superimposing two maxwellian-type distributions in which the exponents  $n$  and  $m$  were varied from  $-1/2$  to 1 in steps of  $1/2$ :

$$\ln\left(\frac{dN}{dE_{\perp}}\right) = \ln\left[\alpha \cdot E_{\perp}^m A(m, T_1) e^{-\frac{E_{\perp}}{k_B T_1}} + \beta \cdot E_{\perp}^n B(n, T_2) e^{-\frac{E_{\perp}}{k_B T_2}}\right] \quad (1)$$

Where  $A(m, T_1)$  and  $B(n, T_2)$  are normalization factors such that  $\int_0^\infty E_\perp^m A(m, T_1) e^{-\frac{E_\perp}{k_B T_1}} dE_\perp = 1$ ,  $\int_0^\infty E_\perp^n B(n, T_2) e^{-\frac{E_\perp}{k_B T_2}} dE_\perp = 1$  and  $\alpha + \beta = 1$ .

The temperatures  $T_1$ ,  $T_2$  of the two distributions and the factors  $\alpha$  and  $\beta$ , were free parameters in the fitting procedure,  $k_B$  is the Boltzman constant.

The best fits to all the energy spectra were obtained with  $m = -1/2$  which corresponds to a one-dimensional maxwellian distribution describing the coolest part of the spectra:

$$F(E_{c\perp}) = \frac{E_\perp^{-1/2}}{\sqrt{\pi k_B T_1}} e^{-\frac{E_\perp}{k_B T_1}} \quad (2)$$

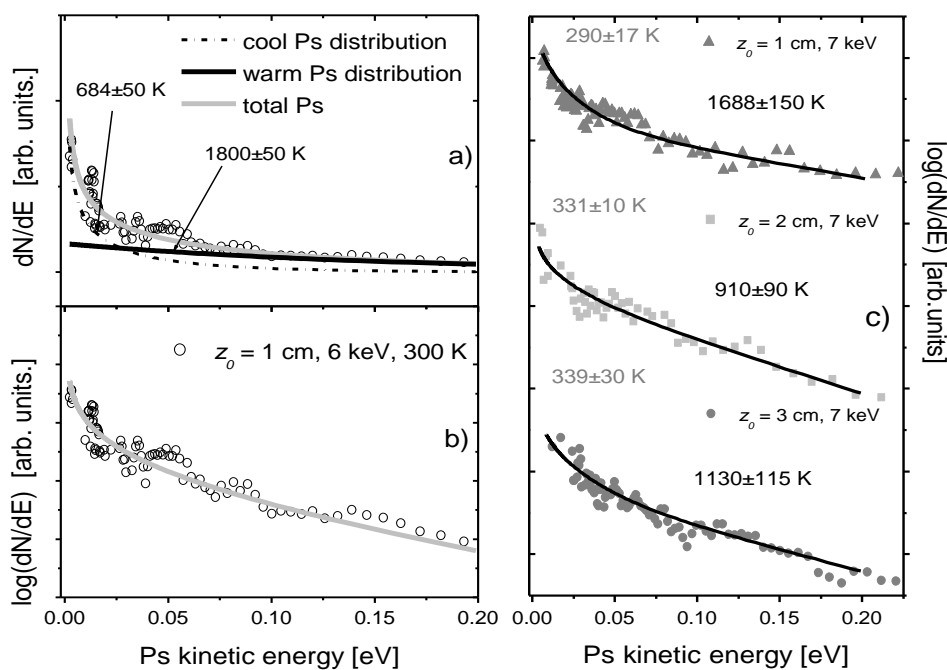


**Figure 2.** a) and b), Ps energy spectrum measured at  $E_+ = 6$  keV and  $z_0 = 1$  cm in linear and semilog scale, respectively. The light gray curves are best fits that result from the sum of a one-dimensional maxwellian and a beam maxwellian distribution as in equation (1). The one-dimensional maxwellian distribution corresponding to the cool Ps fraction and the beam maxwellian distribution corresponding to the warm Ps fraction are reported in a) as dash-dot and continuous black lines respectively. Their characteristic temperatures are also indicated. c) Ps energy spectra, in semilog scale, measured at  $E_+ = 7$  keV and with  $z_0 = 1$  cm, 2 cm, 3 cm. The lines are best fits to the data obtained with equation (1). The characteristic temperatures of the two distributions are extracted from the fits.

whose average kinetic energy is given by  $\langle E_{c\perp} \rangle = \frac{T_1 k_B}{2}$  and with  $n=0$  which corresponds to a beam maxwellian distribution (i.e. a simple exponential function) describing the warm part of the spectra:

$$G(E_{w\perp}) = \frac{1}{k_B T_2} e^{-\frac{E_\perp}{k_B T_2}} \quad (3)$$

whose average kinetic energy is given by  $\langle E_{w\perp} \rangle = T_2 k_B$ . From now on, we will call these distributions, cool distribution and warm distribution of the spectra, respectively.

As the fitting procedure does not support  $\alpha = 0$  or  $\beta = 0$ , a single distribution is not sufficient to describe the energy spectra. A change in the slope of the energy spectra can be appreciated by observing the spectrum measured with  $E_+ = 6$  keV and reported in linear scale in figure 2a. The lines in figure 2 are best fits to the experimental data. In figure 2a, one can notice how the beam maxwellian dominates at higher energy while the one-dimensional maxwellian is crucial to describe the steep slope of the data at lower energy. The fitted temperature  $T_1$  and  $T_2$  characterizing the two distributions are reported.

Increasing the positron implantation energy from 6 to 7 keV, the temperature  $T_1$  of the cool distribution strongly decreases from  $684 \pm 50$  K to  $290 \pm 17$  K, while the temperature of the warm distribution is only reduced from  $1800 \pm 50$  K to  $1688 \pm 150$  K (figure 2c). The spectra measured at  $E_+ = 7$  keV and  $z_0 = 1$  cm, show that a fraction of Ps atoms approaches thermal equilibrium with the sample and is emitted into vacuum at near thermal energies. A more precise evaluation of the temperature requires taking into account the permanence time of Ps inside the sample before being emitted, i.e. the cooling time.

The blue and red curves in figure 3a represent the time distributions relative to the cool and warm energy distributions (equations (2) and (3) respectively) with the weights  $\alpha$  and  $\beta$ , and the temperatures  $T_1$  and  $T_2$  extracted from the fits. In order to determine each time distribution, the corresponding energy distribution is divided by  $t^3$  and multiplied by a normalization coefficient. The gray curves, sum of the red and blue ones, reproduce fairly well the Ps-TOF spectra.

The average time of flight  $\langle t_m \rangle$  was calculated for the cool and the warm component of each time distribution measured at  $z_0 = 1, 2$  and  $3$  cm. This time is the sum of two factors:  $\langle t_m \rangle = \langle t_p \rangle + \langle t_f \rangle$  where  $\langle t_p \rangle$  is the Ps average permanence time in the nanochannels before emission and  $\langle t_f \rangle$  is the real average time of flight  $\langle t_f \rangle = z_0/v_{\perp}$  with  $v_{\perp}$  being the Ps perpendicular velocity not affected by the permanence time.  $\langle t_m \rangle$  values as a function of  $z_0$  were linearly fitted with the equation  $\langle t_m \rangle = \langle t_p \rangle + z_0/v_{\perp}$  and are shown in fig 3b. The intercepts of the two sets of values give  $\langle t_p \rangle = \langle t_{c1} \rangle$  and  $\langle t_p \rangle = \langle t_{c2} \rangle$ , the average Ps cooling time of the cool and warm distribution respectively. The slopes of the two straight lines give the reciprocal of the Ps perpendicular velocities  $1/v_{\perp}$ . The error on  $\langle t_m \rangle$  arises from the the statistical error on the temperature of the two distributions (see figure 2c). The error on  $z_0$  is due to the spatial resolution of  $\sim 8$  mm at the target axis as determined by the geometry of the set-up (see figure 1). It was evaluated as represented by the standard deviation,  $8/\sqrt{3}$  mm, associated to a uniform distribution.

The fit gives an average cooling time  $\langle t_{c1} \rangle = 18 \pm 6$  ns for the Ps emitted with the one-dimensional maxwellian distribution. For the Ps of the warm distribution we can only conclude that the average time  $\langle t_{c2} \rangle$  is estimated to be less than 7 ns. The Ps perpendicular velocities result  $v_{c\perp} = 4.8 \times 10^4 \pm 2 \times 10^3$  m/s and  $v_{w\perp} = 7.4 \times 10^4 \pm 3 \times 10^3$  m/s for the cool and warm distributions respectively.

The real average time of flight,  $\langle t_{fc} \rangle$  and  $\langle t_{fw} \rangle$ , of each spectra are correlated to the Ps perpendicular velocities by the relation:

$$v_{c\perp} = \frac{z_0}{\langle t_{fc} \rangle}, v_{w\perp} = \frac{z_0}{\langle t_{fw} \rangle} \quad (4)$$

In order to estimate the Ps temperature and average kinetic energy we assume that the shape of the  $t_f$  distribution is not altered by the permanence time compared to the measured time of flight  $t_m$  distribution. Thus the average time  $\langle t_{fc} \rangle$  and  $\langle t_{fw} \rangle$  of the two time distributions can be calculated

as  $\langle t_{fc} \rangle = 2.67 \sqrt{\frac{2m_0}{2\pi k_B T_c}} z_0$  and  $\langle t_{fw} \rangle = \sqrt{\frac{\pi 2m_0}{2k_B T_w}} z_0$ . Substituting these expressions in equation (4), the

best estimation of temperatures can be achieved as  $T_c = (2.67)^2 \frac{(v_{c\perp})^2 2 m_0}{2\pi k_B}$  for the cool one-dimensional maxwellian distribution [equation (2)], and  $T_w = \frac{(v_{w\perp})^2 \pi 2 m_0}{2k_B}$  for the warm beam

maxwellian distribution [equation (3)]. The temperatures result to be  $T_c = 342 \pm 25$  K, and  $T_w = 1230 \pm 250$  K. From equations (2) and (3) the corresponding average kinetic energies result to be  $\langle E_{c\perp} \rangle = 15 \pm 1$  meV and  $\langle E_{w\perp} \rangle = 107 \pm 22$  meV. Usually when a single Ps-TOF spectrum at a distance  $z_0$  is recorded, it is implicitly assumed that the permanence time  $t_p$  is negligible compared to  $t_f$ . Nevertheless this simple assumption could lead to an incorrect Ps energy evaluation when Ps is formed deep in a porous sample with small or tortuous pores.

The central value of the cool distribution temperature, evaluated in the spectra measured at different distance from the sample surface, rises from 290 K to 339 K approaching the real

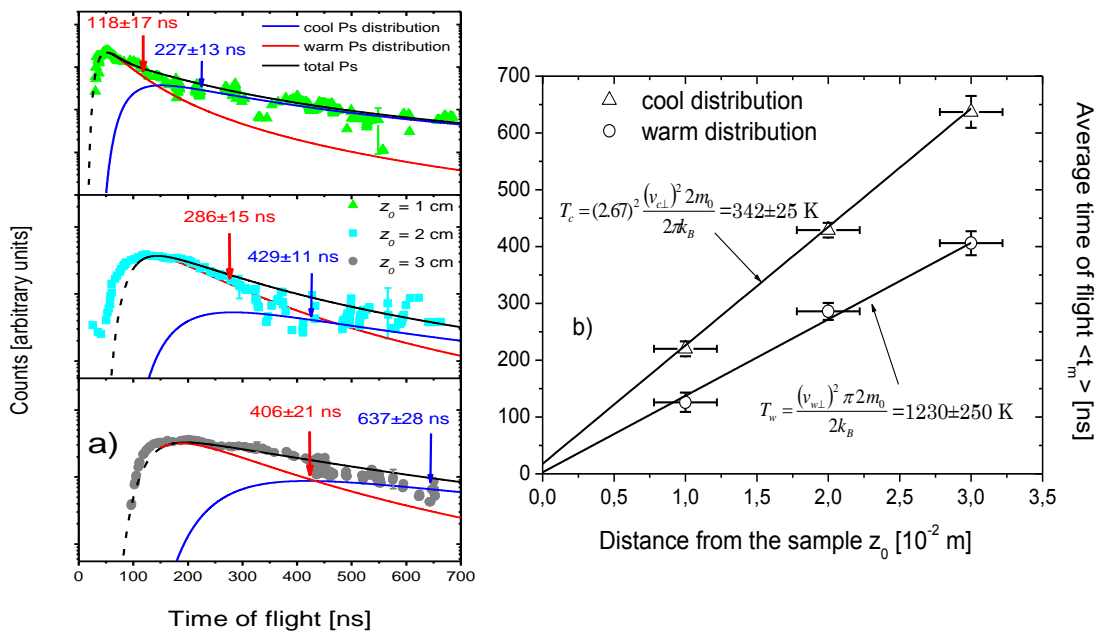


**Figure 3.a)** Ps-TOF spectra measured at  $E_+ = 7$  and at  $z_0 = 1, 2$  and  $3$  cm. The black curves are the time distributions corresponding to the energy spectra best fits. The blue curves are the time distributions of the cool Ps while the red curves are the time distributions of the warm Ps. The average time of flight  $\langle t_m \rangle$  of each distribution is reported and its position marked by an arrow.

**b)** Average time of flight  $\langle t_m \rangle$  calculated from the time distributions of figure 2c, as a function of the distance  $z_0$  from the sample surface. Triangles for cool distributions and circles for warm distributions. The intercepts of the two best fit lines give the mean permanence time  $\langle t_p \rangle$  of Ps before being emitted into vacuum. The slopes of the lines give the perpendicular flying velocity  $v_{c\perp}$  and  $v_{w\perp}$  of the cool and warm Ps distributions.

temperature  $T_c = 342$  K (see figure 2c). As a matter of facts, as the distance  $z_0$  increases, the permanence time  $t_p$  becomes progressively negligible compared to the time of flight  $t_f$ .

From the measured Ps-TOF spectra we can observe that the cool distributions measured at a distance  $z_0 \geq 2$  cm are characterized by a temperature compatible with  $T_c = 342$  K within the errors and are well fitted by a one-dimensional maxwellian function. This is an a posteriori confirmation that, for the present sample, the shape of the distribution is not (or slightly) affected by the permanence time  $t_p$ , as we have previously assumed evaluating  $T_c$ .

The measured  $\langle t_p \rangle = \langle t_{c1} \rangle$  can be compared with a theoretical estimation of permanence time in similar nanochannels calculated in Ref.8. In the framework of the diffusion model, the mean

permanence time of diffusing Ps in 5-8 nm regular nanochannels after  $e^+$  implantation at 7 KeV was calculated to be  $16 \pm 1$  ns [8], in very good agreement with our experimental value of  $18 \pm 6$  ns.

#### 4. Conclusions

We have shown that measuring Ps-TOF spectra at different distances from the surface of a porous sample allows one to extract the cooling time of Ps. From very preliminary measurements done in nanochannelled samples we have estimated a mean Ps cooling time, corresponding to the mean permanence time  $\langle t_p \rangle$  in the nanochannels before emission, of  $18 \pm 6$  ns. In this time Ps reaches quasi thermal kinetic energies  $\langle E_{c\perp} \rangle \cong 15$  meV. The method used to extract  $\langle t_p \rangle$  will allow us to study in detail the cooling process of Ps by measuring  $\langle t_p \rangle$  at different positron implantation energy and at different sample temperature. At present, we have installed an improved version of the Ps-TOF apparatus at the high intensity positron source NEPOMUC inside the FRMII in Munich. First tests with high positron fluxes performed by using a pair of large area MCPs as secondary electron detectors have shown that high signal to noise ratio can be obtained thus largely improving the quality of the data. With this set up more precise results can be obtained by acquiring five spectra at five different distances, in order to validate the linear fitting procedure. In the meanwhile a MonteCarlo simulation is under development in order to understand the origin of the two distributions.

#### References

- [1] Castelli F, Boscolo I, Cialdi S, Giammarchi M G and Comparat D 2008 *Phys. Rev. A* **78** 052512
- [2] Cassidy D B, Hisakado TH, Tom H W K and Mills A P Jr. 2012 *Phys. Rev. Lett.* **108** 043401
- [3] Doser M et al., 2012 *Classical and Quantum Gravity* **29** 184009
- [4] Brusa R S and Dupasquier A 2010 *Physics with many positrons* ed A Dupasquier, A P Mills, Jr. and R S Brusa (IOS Press, Amsterdam, Oxford, Tokio, Washington DC), p. 245.
- [5] Cassidy D B, Crivelli P, Hisakado T H, Liskay L, Meligne V E, Perez P, Tom H W K and Mills A P Jr. 2010 *Phys. Rev. A* **81** 012715
- [6] Mariazzi S, Salemi A and Brusa R S 2008 *Phys. Rev. B* **78** 085428
- [7] Mariazzi S, Bettotti P, Larcheri S, Toniutti L and Brusa R S 2010 *Phys. Rev. B* **81** 235418
- [8] Mariazzi S, Bettotti P and Brusa R S 2010 *Phys. Rev. Lett.* **104** 243401
- [9] Cassidy D B, Hisakado T H, Meligne V E, Tom H W K and Mills A P Jr. 2010 *Phys. Rev. A* **82** 052511
- [10] Macchi C, Mariazzi S, Karwasz G P and Brusa R S, Folegati P, Frabboni S and Ottaviani G 2006 *Phys. Rev. B* **74** 174120
- [11] Di Noto L, Mariazzi S, Bettonte M, Nebbia G and Brusa R S 2012 *Eur. Phys. Jour. D* **66** 118
- [12] Howell R H, Rosenbergl J, Fluss M J, Goldberg R E and Laughlin R B 1987 *Phys. Rev. B* **35** 5303